chemosensors

Article

Perovskite-Structured $NiTiO_3$ Modified NiO Gas Sensor for Xylene Detection

Liyun Qin [1], Hongliang Gao [1] and Fanli Meng [1,2,3,4,*]

[1] College of Information Science and Engineering, Northeastern University, Shenyang 110819, China; 2170766@stu.neu.edu.cn (L.Q.); gaohongliang@ise.neu.edu.cn (H.G.)
[2] Hebei Key Laboratory of Micro-Nano Precision Optical Sensing and Measurement Technology, Qinhuangdao 066004, China
[3] National Frontiers Science Center for Industrial Intelligence and Systems Optimization, Northeastern University, Shenyang 110819, China
[4] Key Laboratory of Data Analytics and Optimization for Smart Industry, Ministry of Education, Northeastern University, Shenyang 110819, China
* Correspondence: mengfanli@ise.neu.edu.cn

Abstract: Xylene gas is highly toxic, can irritate the skin, and is also very harmful to the body. Therefore, it is necessary to prepare sensors that can accurately detect xylene. In this paper, $NiTiO_3$ nanoparticles were synthesized by the hydrothermal method and used to modify NiO, and a $NiTiO_3$-modified NiO ($NiTiO_3$-NiO) nanosheet material was successfully prepared. Its microstructure and internal composition were observed and analyzed by various characterization methods. When detecting 100 ppm xylene gas at the optimum temperature, comparing the response level of the $NiTiO_3$-NiO sensor with that of a pure nickel oxide sensor, the former was 20 times that of the latter, and the sensitivity was greatly improved. In a 100 ppm xylene gas environment, the response level of the sensor reached 21, the minimum detection limit was 1 ppm, and the recovery time was 135.75 s. $NiTiO_3$ is a perovskite-structured material, with many active sites and good catalytic properties that promote redox reactions.

Keywords: xylene; hydrothermal method; gas sensor; perovskite

Citation: Qin, L.; Gao, H.; Meng, F. Perovskite-Structured $NiTiO_3$ Modified NiO Gas Sensor for Xylene Detection. *Chemosensors* **2023**, *11*, 264. https://doi.org/10.3390/chemosensors11050264

Academic Editor: Boris Lakard

Received: 24 March 2023
Revised: 21 April 2023
Accepted: 27 April 2023
Published: 29 April 2023

1. Introduction

Xylene is a volatile organic compound, which is colorless and transparent, insoluble in water, but soluble in ethanol. Xylene gas has certain toxicity, which is irritating to the skin and mucous membranes. Wallpaper, paints, coatings, and dyes used in decoration generally contain xylene, which is also an important raw material for organic chemicals. In general, breathing under the condition of xylene concentrations greater than 200 mg/m^3 air for 8 h will produce poisoning symptoms [1,2]. Long-term use will do great harm to the body [3–5]. Therefore, it is very urgent and necessary to find a rapid and accurate method for detecting xylene. So far, many detection methods have been used to detect xylene, such as spectroscopy, biosensors, and gas sensors. Among them, the gas sensor method is very common [6–8]. Gao et al. [9] prepared Sn-doped NiO hierarchical structures via the hydrothermal method to detect xylene. Li et al. [10] successfully prepared Au nanoparticles loaded with WO_3 nanoflower materials for the detection of xylene, using a hydrothermal method.

Semiconductor gas sensors based on metal oxide materials are widely used due to their series of advantages, such as high sensitivity, low production cost, and portability [11]. It is well known that the sensors with n-type material properties have greater response values than semiconductor gas sensors with morphological p-type materials. However, the types of gases that can be clearly distinguished by sensors based on n-type materials are still limited, mainly because the selectivity of the sensors needs to be improved [12–15].

NiO, which is common in p-type materials, is used in this paper. Shailja et al. [16] prepared an Al-doped NiO sensor, and the response value of the sensor to 10 ppm toluene could reach 29 at 180 °C. Gao et al. [17] made a SnO_2-modified NiO sensor to detect 100 ppm toluene with a response value of 66.2 and a minimum detection limit of 10 ppb. NiO is a p-type semiconductor material, and sensors made of NiO have high catalytic activity for VOCs [18]. It has a wide band gap range and is adjustable. In addition to this, it is chemically very stable [19–21]. NiO has been found to have outstanding catalytic activity during the oxidation of volatile organic compounds [22]. NiO has a catalytic effect on redox reactions. Its catalytic activity is very high, which makes it an excellent sensor for detecting VOC gases [23–25]. It has excellent performance when used as a gas sensor. However, a sensor made of pure NiO also has disadvantages, such as low response value. Feng et al. [26] prepared NiO nanotubes to detect xylene, and the response value of pure NiO nanotubes to 200 ppm gas was below 3.1. Chen et al. [27] used a pure NiO sensor to detect 100 ppm toluene and xylene at 230 °C, and the response value was less than 2.

Therefore, other materials are considered for use to improve performance [28,29]. The general structural formula of perovskite materials can be summarized as ABO_3, where divalent cations usually exist at site A and tetravalent cations usually exist at site B. The type and radius of the ions at A and B sites will affect the overall structural stability [30,31]. Perovskite materials have a high optical absorption coefficient and high carrier mobility. The appearance and change of cation vacancies in perovskite structured materials can provide space for gas adsorption. Perovskite structural materials contain a large number of oxygen vacancies, which can adsorb or desorb a large amount of oxygen and promote redox reactions. Perovskite structural materials have high catalytic activity [32,33], and $NiTiO_3$ is a typical perovskite structure material, which has great research prospects and potential. $NiTiO_3$ materials are widely used in batteries and photocatalysis [34,35]. In past studies, few people have combined titanium-based perovskite materials with NiO materials. $NiTiO_3$ has good catalytic activity. It is low-cost and easy to obtain. It has great application value in photocatalysis, gas sensors, cathode materials for lithium-ion batteries, and so on [36].

In this paper, nickel titanate-modified nickel oxide materials were successfully synthesized by the hydrothermal method. The materials prepared by this method combined the advantages of $NiTiO_3$ and NiO. The addition of $NiTiO_3$ greatly improved the performance of NiO sensors.

2. Materials and Experimental Details

2.1. Materials Overview

All reagents, such as methenamine, $Ni(NO_3)_2{\cdot}6H_2O$, $C_{16}H_{36}O_4Ti$, ethylene glycol and so on, could be used without further purification. The water used throughout the experiment was ultrapure.

2.2. Synthesis Methods

In total, 20 mL ethylene glycol was added to 10 mL water and stirred well. Then, 0.56 g methenamine and 0.58 g $Ni(NO_3)_2{\cdot}6H_2O$ were added into the solution and stirred for 0.5 h. We poured the solution into the reactor and put it into the oven manufactured by Shanghai Yiheng, setting the oven temperature to 150 °C for 4 h. At the end of the reaction, the reactants were poured into centrifuge tubes and centrifuged, then dried after washing several times with water and ethanol. The dried material was baked in an oven at 60 °C. Finally, the material was calcined, and the muffle furnace used in this process was made by Shanghai Yiheng. As shown in Figure 1, the sample was roasted in a Muffle furnace at 800 °C for 2 h to obtain unmodified NiO.

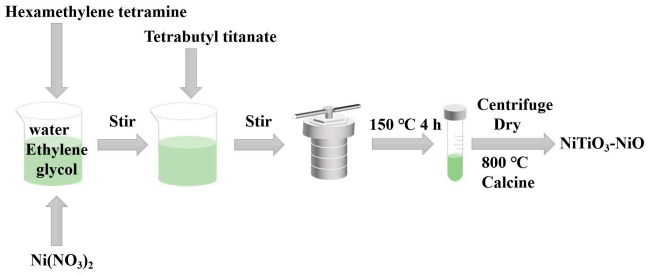

Figure 1. Experimental process diagram of preparing $NiTiO_3$-NiO material.

We repeated the process described in B, adding tetrabutyl titanate (2 at%, 10 at%, 25 at%) to the process, and then poured the solution into the reactor with the temperature and duration set as above. After the end of the reaction, centrifugation and drying were performed. The drying temperature was 60 °C. Finally, the sample was put into a muffle furnace and calcined at 800 °C for 2 h. $NiTiO_3$-NiO could be obtained.

2.3. Summary of Characterization Methods

Firstly, the material was scanned by XRD and compared with the standard card to determine the kind of material. The morphologies of NiO and $NiTiO_3$-NiO samples were observed by SEM, and the composition and proportion of elements were observed by EDS. Then, the internal structure was observed by TEM, and the valence state of elements in the material was examined by XPS.

2.4. Gas Sensing Performance Data Test Platform

The sensor model used in the experiment is shown in Figure 2. Before testing the properties of the sensor, the material should be coated on the ceramic tube of the sensor. The base of the sensor was made of rubber, and the base was inserted into the bottom of the air chamber during the test. The length of the ceramic tube was approximately 4 mm, the diameter was about 1 mm, the spacing between the gold electrodes was approximately 2 mm, and the resistance value of the resistance wire used was 30 Ω. During the heating process, the resistance value remained unchanged. In total, 2 mg $NiTiO_3$-NiO material was put into a 1.5 mL reagent tube, then 5 uL of anhydrous ethanol was added to the tube, and the reagent tube was placed on the upper part of the shaker to disperse the mixture until it was gel-like, and the gel-like mixture was evenly coated on the sensor by pipetting with a pipette, so that the coated material had a uniform thickness and smooth surface, and the coated sensor was well marked. The thickness of the material on the sensor was 1503 um and the surface was smooth. Four sets of experiments were done. When testing the data, three sensors were prepared for each set of experiments, and multiple repeatable measurements were made. The material was applied evenly every time, so there was not much difference in the equipment. The details of the test platform can be seen in Figure 2. The rubber base of the sensor contained six electrodes, which were connected to the top of the platinum electrodes and both ends of the resistance wires. The two electrodes welded together with the resistance wire were connected to a DC power supply, and the temperature applied to the sensor could be adjusted by controlling the power supply. The digital source meter was connected with four platinum wires, and the resistance changes of the sensor were transmitted to the computer through Labview software. The air chamber had an air inlet and an outlet, and before each test, the valve connecting the air chamber was opened, the synthetic air inside the cylinder entered the gas chamber through the valve, and after the reaction was stable, the valve was opened to completely drain the gas. This ensured that the environmental conditions were the same for each test and that the air was clean. The gas sensor was placed in the cube in Figure 2, and various test gases were introduced into it through the syringe. After the gas measurement was completed, synthetic air was blown into it to discharge the organic gas. In this paper, the sensor was measured using a current source with a current set at 1×10^{-8} A. The response value of

the gas sensor is represented by S, and S is the ratio of the resistance values of the sensor. The resistance was high in the target gas and low in the air.

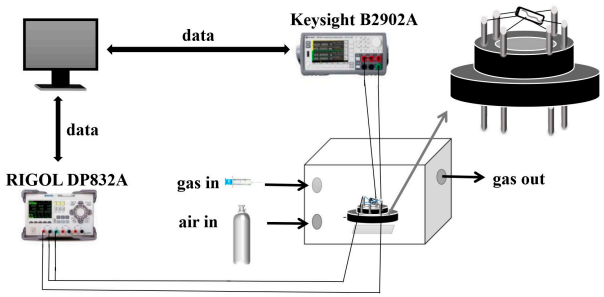

Figure 2. Schematic of the gas sensor and the testing device.

3. Characterization Results and Data Analysis

3.1. Characterizations

Figure 3 shows the SEM diagram for characterizing the microscopic morphology of the product. It could be seen from Figure 3a that the prepared NiO had a large blocky structure and uneven distribution. Figure 3b is the SEM image of $NiTiO_3$ added to the NiO sample with an atomic ratio of 2%. This sample had a lamellar structure composed of particles, and a large gap could be observed in the middle. In Figure 3c, the 10% $NiTiO_3$-NiO sample particles were combined to form a lamellar structure with a smaller and more uniform gap in the middle, while in Figure 3d, 25% $NiTiO_3$-NiO samples formed a lamellar structure with particles tightly combined. Under the same synthesis conditions, the morphology of the 10% $NiTiO_3$-NiO sample was more regular, uniform, and dispersed, and the active sites were further increased, which was beneficial to increasing the gas diffusion path, shortening the reaction time and improving the gas characteristics of the sensor. In order to further analyze its microstructure and phase composition, HRTEM was used to analyze it. The HRTEM image of the 10% $NiTiO_3$-NiO sample is shown in Figure 3e, which distinguished different lattice planes. The (200) and (111) lattice spacing of NiO were 0.21 nm and 0.24 nm, respectively, and the (110) lattice spacing of $NiTiO_3$ was 0.25 nm. This is in good agreement with the results of the XRD analysis.

Figure 4 shows the uniform distribution of elements O, Ni, and Ti in the 10% $NiTiO_3$-NiO samples. The above results were consistent with the outcomes of EDS and XRD.

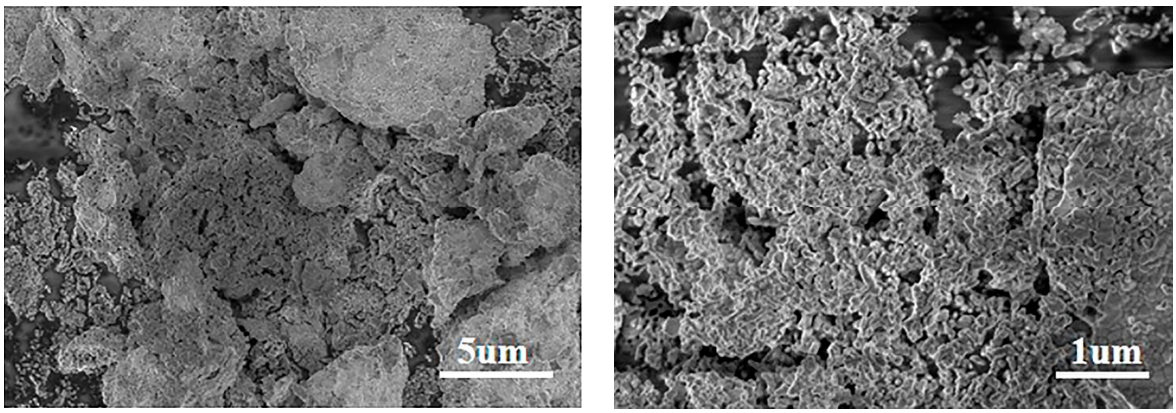

(**a**) (**b**)

Figure 3. *Cont.*

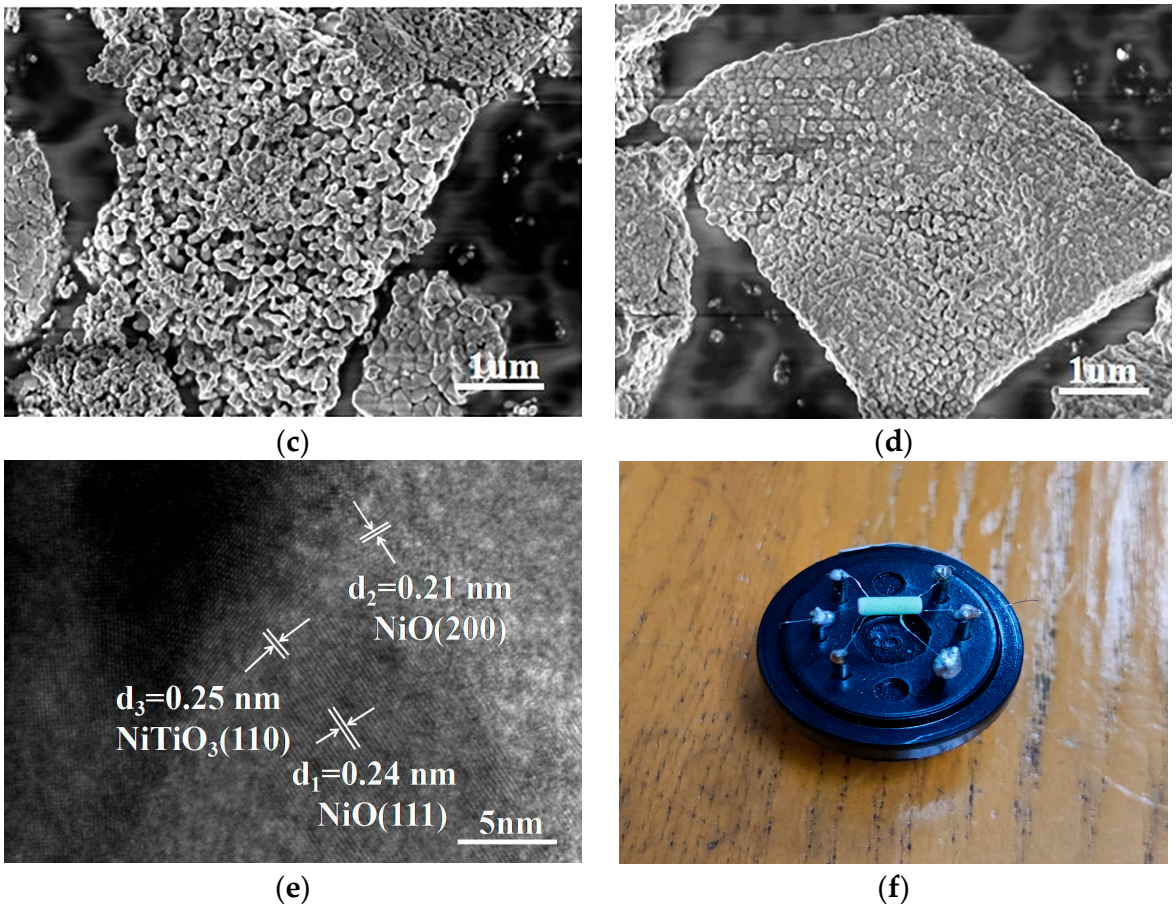

Figure 3. SEM images of (**a**) NiO; (**b**) 2% $NiTiO_3$-NiO; (**c**) 10% $NiTiO_3$-NiO; (**d**) 25% $NiTiO_3$-NiO. HRTEM image of (**e**) 10% $NiTiO_3$-NiO. (**f**) Physical image of NiO sensor.

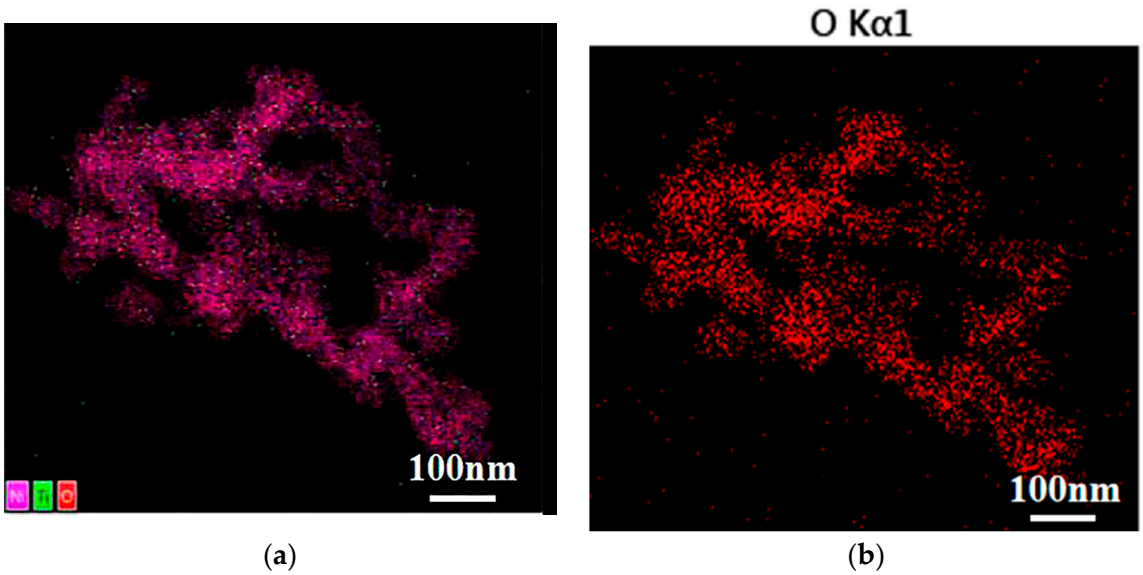

Figure 4. *Cont.*

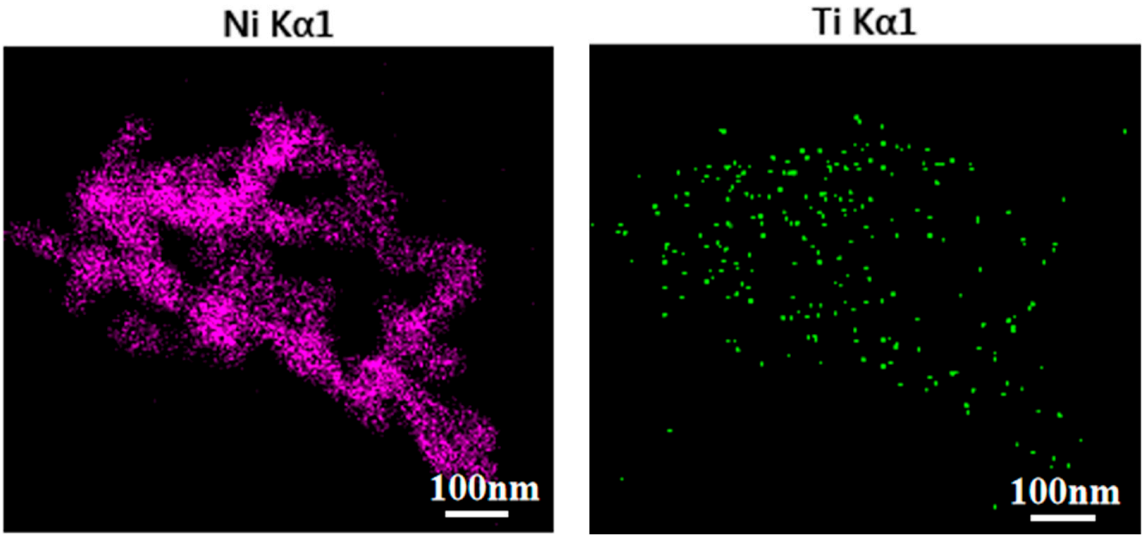

Figure 4. Elemental mapping images of 10% $NiTiO_3$-NiO (**a**) O, Ni, and Ti; (**b**) O; (**c**) Ni; (**d**) Ti.

In Figure 5a, we can see the XRD figures of the prepared NiO and $NiTiO_3$-NiO. Among them, diffraction peaks (111) and (200) corresponded to JCPDS card No. 71-1179 at 2θ angles of 37.245° and 43.275°. The diffraction peak (110) in the sample corresponded to the spectrum of nickel titanate. In addition, no other diffraction peaks were found, which indicates that the synthesized samples were of high purity.

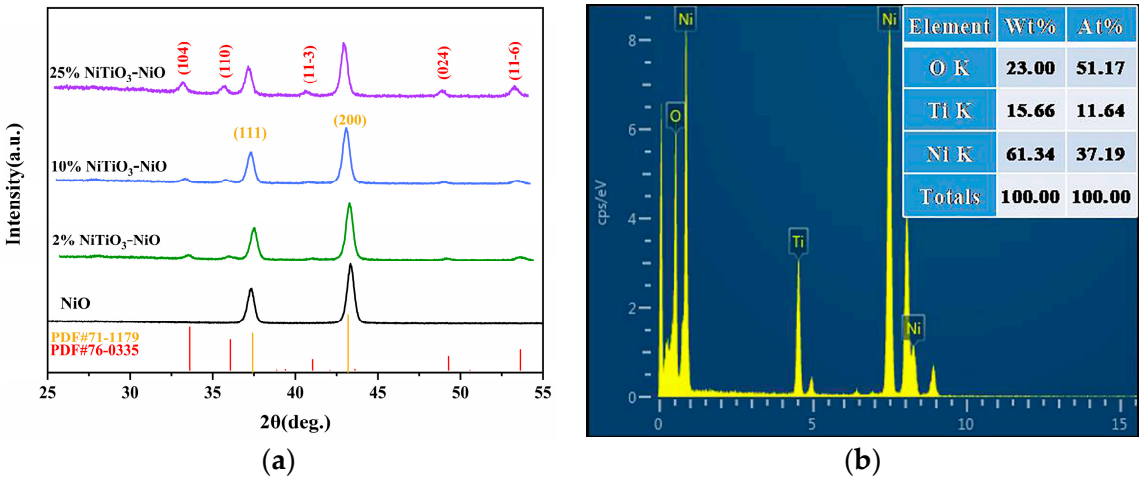

Figure 5. (**a**) XRD images of pure NiO, 2% $NiTiO_3$-NiO, 10% $NiTiO_3$-NiO, and 25% $NiTiO_3$-NiO; (**b**) EDS analysis of the 10% $NiTiO_3$-NiO.

In the XRD diagram of $NiTiO_3$-NiO, the diffraction peaks of $NiTiO_3$ can be seen, which also matched with JCPDS card No. 76-0335. When the content of $NiTiO_3$ added to the material increased, the diffraction summit of $NiTiO_3$ gradually sharpened. Adding $NiTiO_3$ did not destroy the lattice structure of NiO. The XRD patterns of 2% $NiTiO_3$-NiO, 10% $NiTiO_3$-NiO, and 25% $NiTiO_3$-NiO showed the diffraction peaks of NiO, which were matched with NiO (JCPDS card No. 71-1179). No other obvious impurity peaks were detected.

The chemical composition of the material was analyzed by EDS, as shown in Figure 5b. The results show that 10% $NiTiO_3$-NiO fully contained O, Ni, and Ti elements, and there was no interference from other clutter elements. The content percentages of O, Ni, and Ti elements are shown in Figure 5b.

The valence state and elemental composition of the compounds were determined by XPS. Calibration was performed with carbon-contaminated C1s (284.8 eV). The XPS measurement of 10% $NiTiO_3$-NiO can be seen in Figure 6. It can be seen from Figure 6a that NiO was composed of Ni and O elements, and the 10% $NiTiO_3$-NiO material was composed of Ni, Ti, and O elements.

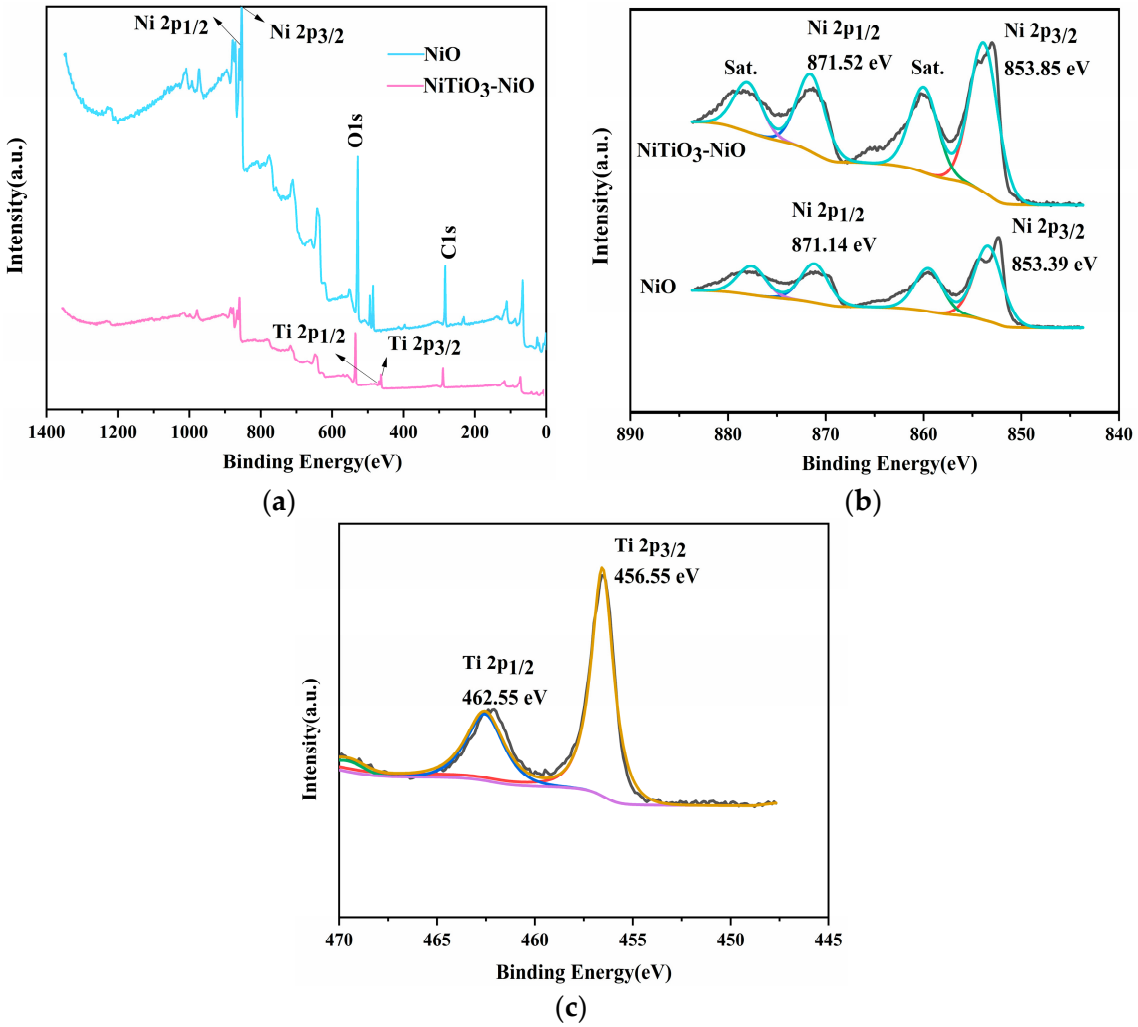

Figure 6. XPS spectra of (**a**) NiO and 10% $NiTiO_3$-NiO; (**b**) Ni 2p; (**c**) Ti 2p.

As shown in Figure 6b, the Ni 2p spectrum of pure NiO had two main peaks at 871.14 eV and 853.39 eV. Due to spin site splitting, the two peaks belonged to Ni $2p_{1/2}$ and Ni $2p_{3/2}$, respectively. The peak binding energies of Ni $2p_{1/2}$ and Ni $2p_{3/2}$ in 10% $NiTiO_3$-NiO samples were 871.52 eV and 853.85 eV, respectively, while those in pure NiO samples were 871.14 eV and 853.39 eV, respectively. There were two main peaks in the Ti 2p spectrum of 10% $NiTiO_3$-NiO. Due to spin site splitting, the two peaks belonged to Ti $2p_{1/2}$ and Ti $2p_{3/2}$, respectively. The Ti $2p_{1/2}$ and Ti $2p_{3/2}$ binding energy peaks were 462.55 eV and 456.55 eV, respectively. After adding $NiTiO_3$, the peak value of binding energy shifted, which was the result of electronic interaction.

3.2. Gas Sensing Properties

Xylene was used as the main detection gas. The sensitive characteristics of the sensor were closely related to the working temperature. Therefore, the most suitable temperature for sensor operation should be determined before studying the gas response characteristics of NiO. The response values of the four sensors to 100 ppm xylene gas between 275 °C and 400 °C could be seen in Figure 7a.

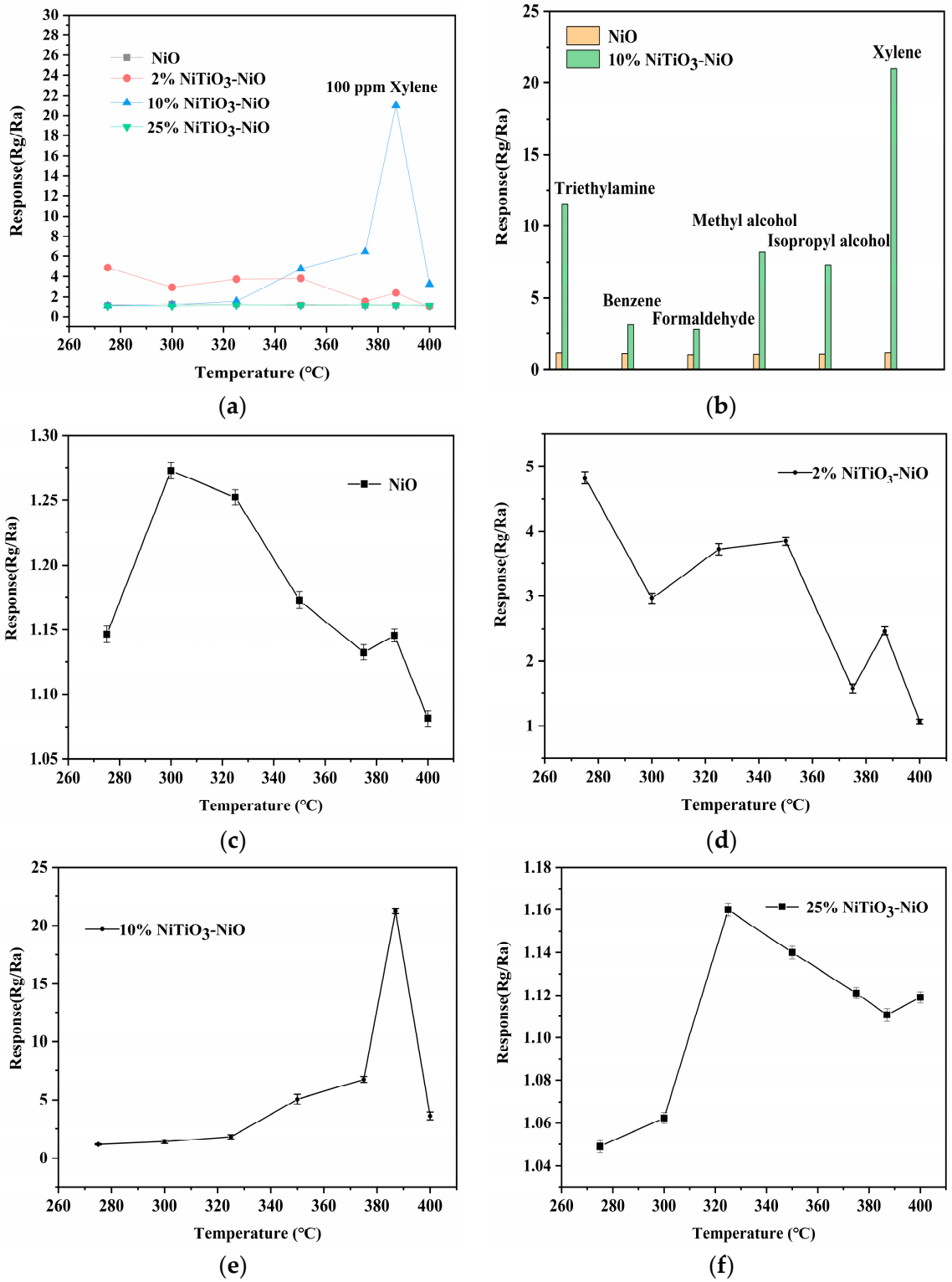

Figure 7. (**a**) Optimal operating temperature curves for NiO, 2% $NiTiO_3$-NiO, 10% $NiTiO_3$-NiO, and 25% $NiTiO_3$-NiO sensors. (**b**) Response of NiO and 10% $NiTiO_3$-NiO sensors to different gases at 100 ppm. Optimal operating temperature curves for (**c**) NiO; (**d**) 2% $NiTiO_3$-NiO; (**e**) 10% $NiTiO_3$-NiO; (**f**) 25% $NiTiO_3$-NiO sensors.

As shown in Figure 7a, the curve of 10% $NiTiO_3$-NiO rose and then decreased, with the highest response value at 387 °C. The main reason was that when the operating temperature was poor, the xylene gas molecules were underactive, and did not get enough energy for the

reaction. As the operating temperature increased, the surface reaction between xylene and the oxygen adsorbed on the surface was accelerated, leading to an increase in the response value. However, when the temperature was too high, the xylene molecule received too much energy and the vibration caused it to be difficult to adsorb on the sensor surface, causing the response value to decrease. The maximum response value at 387 °C reached 23, which was much higher than that of unmodified NiO (1.13). The sensitivity of the material to xylene was significantly improved after modification with $NiTiO_3$. In Figure 7a, the results suggest that the presence of $NiTiO_3$ could greatly improve the performance of the NiO sensor in detecting xylene, which might be due to the more uniform internal distribution and larger specific surface area of the 10% $NiTiO_3$-NiO sensor. This improved performance might be due to the introduction of $NiTiO_3$, which increased the average pore size of the 10% $NiTiO_3$-NiO sensor so that oxygen molecules and xylene gas molecules could enter the material more quickly and promote the reaction.

In addition, the sensitivity of two sensors to different VOC gases at the optimum operating temperature was also investigated, as shown in Figure 7b, including triethylamine, benzene, formaldehyde, methyl methanol, isopropanol, and xylene. It could be seen from the figure that the 10% $NiTiO_3$-NiO sensor was more sensitive to xylene than the other gases. The 10% $NiTiO_3$-NiO sensor showed a great improvement in sensing performance for xylene gas, while the response to other gases did not change much. The response values of pure NiO sensors did not vary much for different target gases, which was due to the strong cross-sensitivity of the sensors. The 10% $NiTiO_3$-NiO sensor widened the gap of response values between xylene and other gases while improving the response values, and $NiTiO_3$ reduced the cross-sensitivity of the original NiO sensor.

In addition, based on the excellent performance of the 10% $NiTiO_3$-NiO sensor for xylene gas, its dynamic response curves for different ppm xylene gases were also investigated in Figure 8. When the xylene gas concentration increased, the response value of the sensor also increased. In addition, the results were fitted. The relationship between gas concentration and response value was linear, which shows that the sensor had a great positive detection range and good stability.

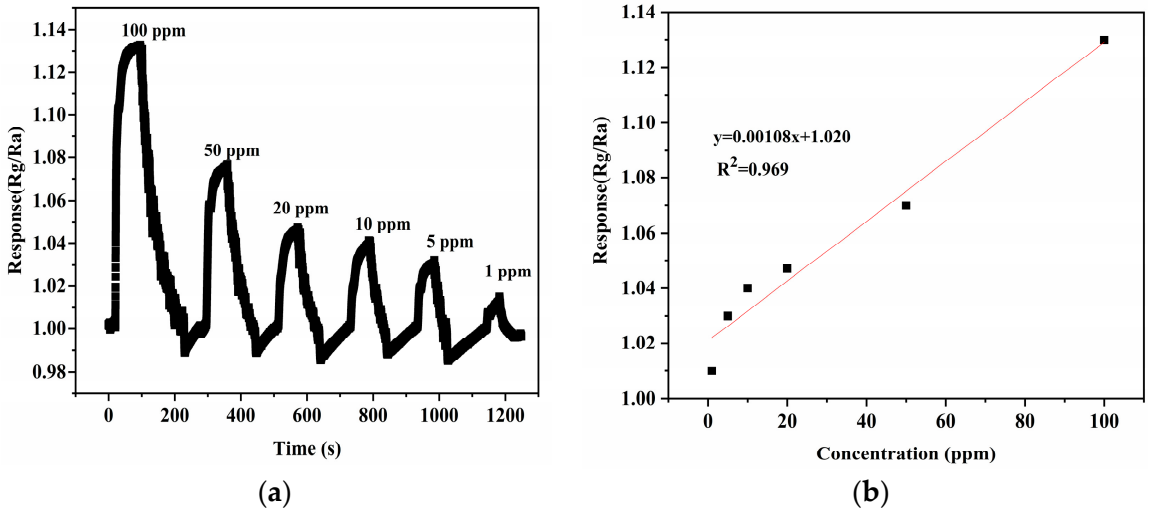

(**a**) (**b**)

Figure 8. *Cont.*

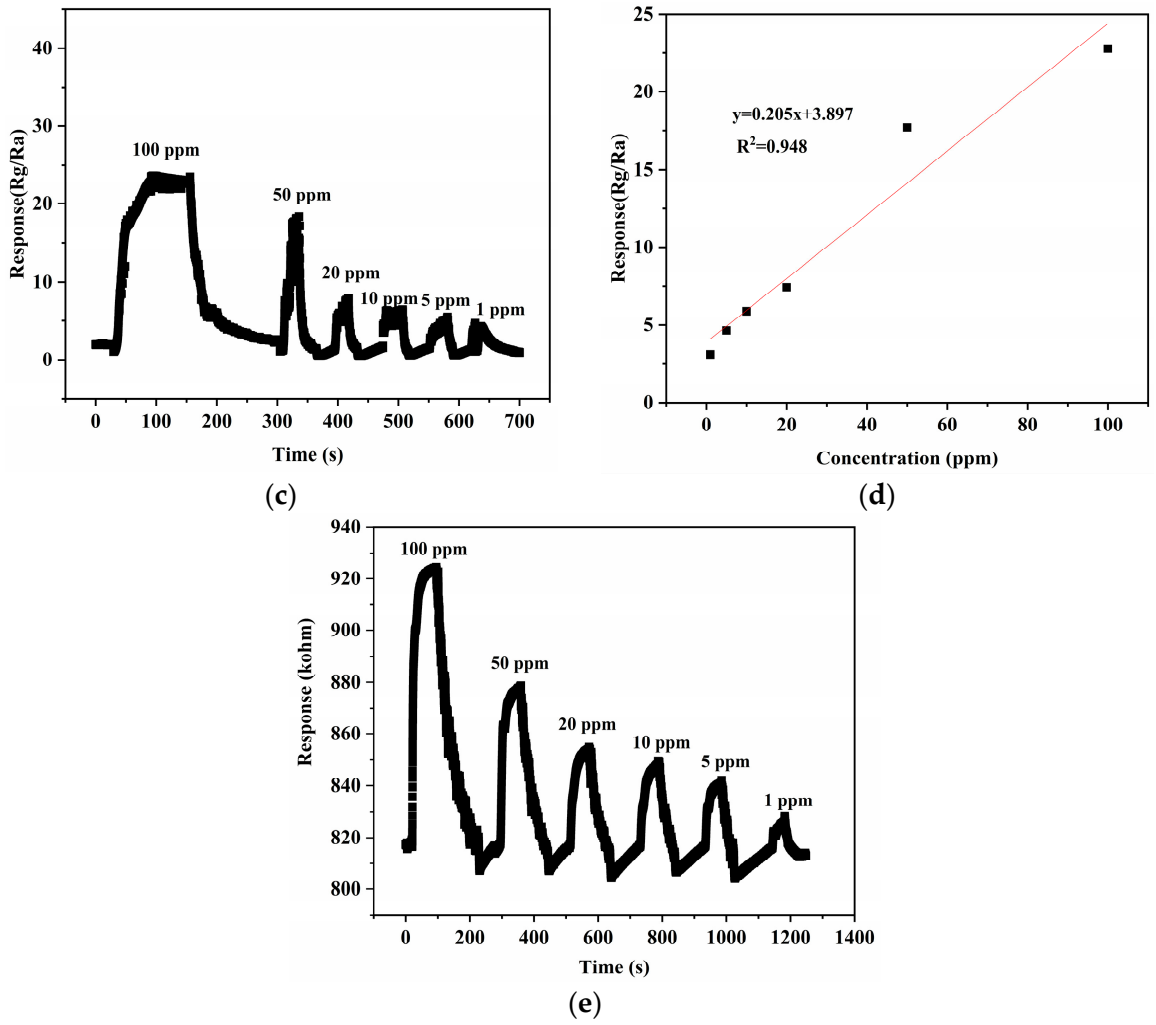

Figure 8. (**a**) Dynamic response curves to different concentrations of NiO. (**b**) The fitting curve of NiO responses to different concentrations of xylene gas. (**c**) Dynamic response curve to different concentrations of 10% $NiTiO_3$-NiO. (**d**) The fitting curve of 10% $NiTiO_3$-NiO responds to different concentrations of xylene gas. (**e**) Raw resistance response curve of 10% $NiTiO_3$-NiO.

In Figure 9b, we can see the repeatability test curve of a 10% $NiTiO_3$-NiO sensor for 100 ppm xylene gas. After many cycles of testing, the resistance of the 10% $NiTiO_3$-NiO sensor had no obvious attenuation. At 100 ppm xylene gas, the sensor's response value was almost constant. The response time and recovery time changed little in each process, which indicates that the continuity of the sensor was great. After calculation, the recovery time of the sensor was 135.75 s and the response time was 133.5 s. As shown in Figure 9c, repeated sensing performance measurements on xylene gas at 100 ppm for one month were performed to estimate the effectivity of the 10% $NiTiO_3$-NiO sensor. It was found that the gas sensing response of the sensor maintained good stability, staying above 20. This stable and good characteristic lays a solid foundation for $NiTiO_3$-NiO to be a good candidate material for xylene detection in the future.

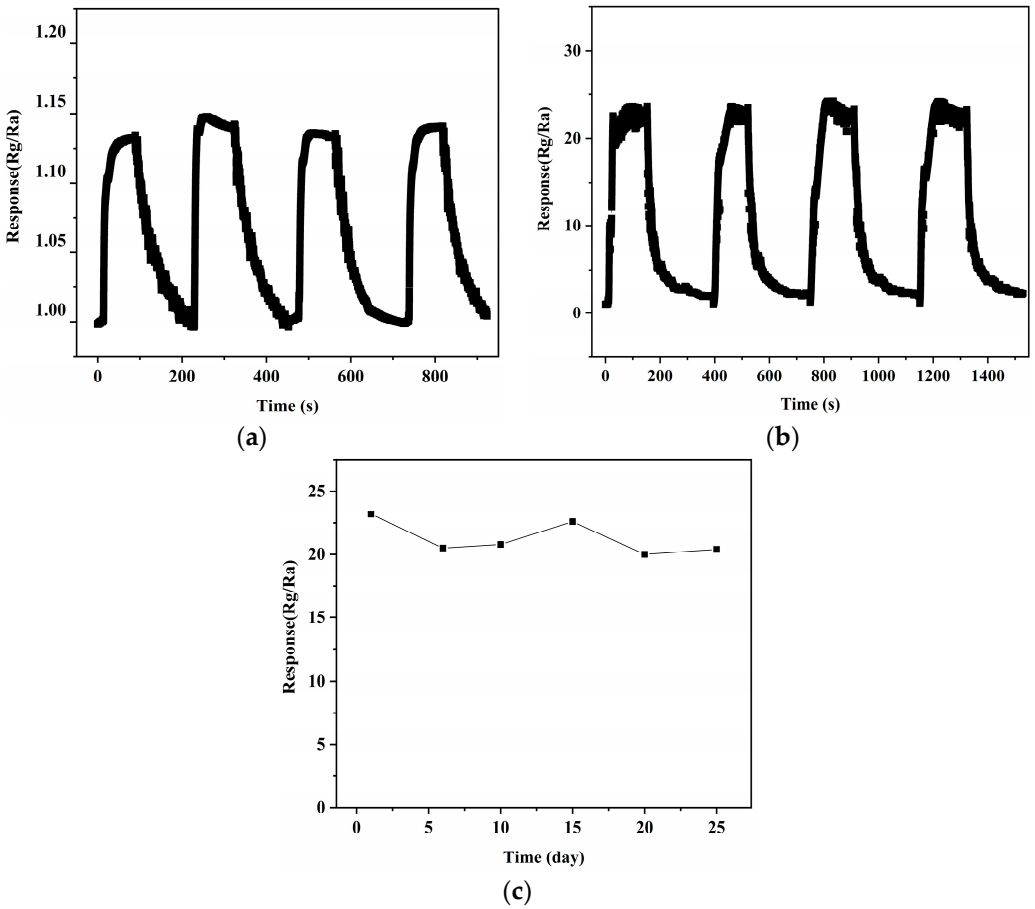

Figure 9. (**a**) Repeatability measurement curve of NiO. (**b**) Repeatability measurement curve of 10% $NiTiO_3$-NiO. (**c**) Stability measurement curves of 10% $NiTiO_3$-NiO.

The sensitivity of the 10% $NiTiO_3$-NiO sensor was greatly improved, and its selectivity was outstanding. Moreover, the continuity of the sensor was excellent, and after a long time, it could still maintain good stability. However, the recovery time and response time were relatively long; the sensor could react quickly to the gas, but it took some time to reach the equilibrium state of response, and this could be improved in the future to make it respond and recover quickly.

The xylene gas sensing performance of the prepared $NiTiO_3$-NiO gas sensor was compared with the previously studied materials, and the results are shown in Table 1.

3.3. Gas Sensing Mechanism

NiO is classified as a p-type semiconductor material, and its gas sensing mechanism can be explained by the space charge layer model. When the NiO or $NiTiO_3$-NiO sensor was in the air, molecules of oxygen adsorbed on the material would cause electrons in the conduction band to be transferred and form different types of oxygen ions (O^{2-}, O^{-}, O_2^{-}), forming a whole accumulation layer on the surface of NiO, and reducing the resistance. When xylene was detected, the xylene molecules reacted with adsorbed oxygen-negative ions, releasing electrons back into the material, thus reducing the carrier concentration and increasing the resistance. The reaction process was as follows [37,38]:

$$O_2(gas) \rightarrow O_2(ads) \quad (1)$$

$$O_2(ads) + 4e^{-} \rightarrow 2O^{2-}(ads) \quad (2)$$

$$(C_6H_4CH_3CH_3)ads + 21O^{2-}(ads) \rightarrow 8CO_2(gas) + 5H_2O(gas) + 42e^- \quad (3)$$

On the other hand, for the $NiTiO_3$-NiO material, the reason for the improvement in gas sensing performance was the existence of the p-n heterojunction [39–41]. As shown in Figure 10, when the p-type material NiO and the n-type material $NiTiO_3$ contacted each other, a p-n heterojunction would be formed. Between NiO and $NiTiO_3$, holes and electrons would move in opposite directions; holes would move from the surface of NiO to $NiTiO_3$, and electrons would move from the surface of $NiTiO_3$ to NiO. This caused the band near the surface of NiO to bend downward, and the band near the surface of $NiTiO_3$ to bend upward, eventually reaching an equilibrium Fermi level. Therefore, an electric field was formed in the space charge layer where NiO and $NiTiO_3$ were contacted. The holes on the surface of NiO would be neutralized with the electrons on the surface of $NiTiO_3$. Finally, the electron depletion layer would be formed at the junction of NiO and $NiTiO_3$, which would further increase the amount of adsorbed oxygen. As such, when the material was in contact with xylene gas, more electrons would be released back into the composite, improving its properties.

Table 1. Xylene gas sensors that have been reported.

Materials	Concentration (ppm)	Temperature (°C)	Response (Rg/Ra)	Response Time/Recovery Time (s)	Reference
2 at% W-NiO	200	375	8.7	178/152	[26]
$NiGa_2O_4$-NiO	100	230	16.3	-	[27]
0.5 at% Ag/TiO_2	100	375	6.5	5/2	[42]
In-doped ZnO	100	420	10.1	-	[43]
α-MoO_3/α-Fe_2O_3	100	206	6.9	87/190	[44]
10% α-Fe_2O_3/Bi_2WO_6	100	260	13.5	20/40	[45]
10% $NiTiO_3$-NiO	100	387	24	31/148	this work

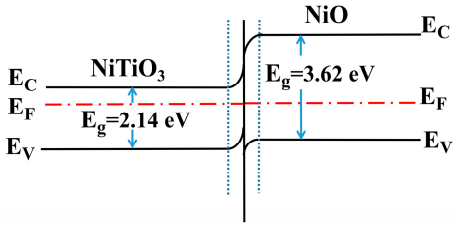

Figure 10. Energy band schematic diagram of $NiTiO_3$-NiO.

The catalytic ability of $NiTiO_3$ with a perovskite structure also contributed to its improved performance. In the field of catalysis, $NiTiO_3$ is a new excellent catalytic material with extremely strong catalytic activity that can promote the redox reaction. The sensing performance was very much improved at the same operating temperature, and this improved performance was mainly due to the catalytic effect of $NiTiO_3$ modification. When xylene molecules were adsorbed on the surface of the catalyst material, they reacted with oxygen that was not chemisorbed in the oxygen vacancy, and eventually, carbon dioxide and water were generated and separated from the surface of the material. On the other hand, Ti ions have a defective catalytic effect, and the large numbers of defects in perovskite-type $NiTiO_3$ provide very good conditions for catalysis. In the structure of perovskite-type materials, the B site is usually a transition metal element, which acts as the position with activity. Its valence state is usually mixed, and it generally will have very strong oxidizing or reducing properties.

Moreover, the addition of $NiTiO_3$ increased the specific surface area of the material, which led to an increase in oxygen adsorption sites and promoted the reaction. The increased oxygen molecular content adsorbed on the material surface could accelerate

the combination with xylene molecules, and the redox reaction was accelerated, which eventually led to a great improvement in the sensing performance of the material. Further, the addition of $NiTiO_3$ led to a large increase in adsorption sites, which increased the adsorption of xylene, and the selectivity of the sensor to xylene was improved.

4. Conclusions

In this paper, nickel oxide materials modified with nickel titanate were successfully prepared via the hydrothermal method, and the microscopic morphology and properties of the materials were analyzed by a series of characterization methods. The presence of trace amounts of nickel titanate was also confirmed. At an optimal temperature of 387 °C, the 10% $NiTiO_3$-NiO sensor had a high response to 100 ppm xylene gas—up to 20 times that of the pure nickel oxide sensor. In addition, it had good selectivity and was stable. The improvement in $NiTiO_3$-NiO sensor performance could be mainly attributed to the surface oxygen adsorption, heterojunction effect, and high catalytic activity of the perovskite-type structural material. As a gas sensing material for the detection of xylene gas, $NiTiO_3$-NiO has great potential and application prospects.

Author Contributions: Conceptualization, F.M.; methodology, L.Q.; validation, H.G. and F.M.; formal analysis, H.G.; investigation, L.Q.; resources, F.M.; data curation, H.G.; supervision, F.M. and H.G.; writing—original draft preparation, L.Q.; writing—review and editing, L.Q.; visualization, L.Q.; funding acquisition, F.M.; project administration, H.G. All authors have read and agreed to the published version of the manuscript.

Funding: This work was supported by the National Natural Science Foundation of China (62071112, 62033002, and 62271006), the Fundamental Research Funds for the Central Universities in China (N2201008), the 111 Project (B16009), the Hebei Natural Science Foundation (F2020501040).

Institutional Review Board Statement: Not applicable.

Informed Consent Statement: Informed consent was obtained from all subjects involved in the study.

Data Availability Statement: Data of our study are available upon request.

Conflicts of Interest: The authors declare no conflict of interest.

References

1. Wang, M.; Varma, R.; Venables, D.S.; Zhou, W.; Chen, J. A Demonstration of Broadband Cavity-Enhanced Absorption Spectroscopy at Deep-Ultraviolet Wavelengths: Application to Sensitive Real-Time Detection of the Aromatic Pollutants Benzene, Toluene, and Xylene. *Anal. Chem.* **2022**, *94*, 4286–4293. [CrossRef]
2. Yang, F.; Ma, J.Z.; Zhu, Q.; Ma, Z.L.; Wang, J. Aggregation-Induced Luminescence Based UiO-66: Highly Selective Fast-Response Styrene Detection. *ACS Appl. Mater. Interfaces* **2022**, *14*, 22510–22520. [CrossRef]
3. Wang, D.; Cheng, Y.; Wan, K.C.; Yang, J.L.; Xu, J.C.; Wang, X.Y. High efficiency xylene detection based on porous MoO_3 nanosheets. *Vacuum* **2020**, *179*, 109487. [CrossRef]
4. Kim, B.Y.; Ahn, J.H.; Yoon, J.W.; Lee, C.S.; Kang, Y.C.; Abdel-Hady, F.; Wazzan, A.A.; Lee, J.H. Highly Selective Xylene Sensor Based on NiO/$NiMoO_4$ Nanocomposite Hierarchical Spheres for Indoor Air Monitoring. *ACS Appl. Mater. Interfaces* **2016**, *8*, 34603–34611. [CrossRef]
5. Gao, H.Y.; Guo, J.; Li, Y.W.; Xie, C.L.; Li, X.; Liu, L.; Chen, Y.; Sun, P.; Liu, F.M.; Yan, X.; et al. Highly selective and sensitive xylene gas sensor fabricated from NiO/$NiCr_2O_4$ p-p nanoparticles. *Sens. Actuators B Chem.* **2019**, *284*, 305–315. [CrossRef]
6. Wang, H.; Chen, M.; Rong, Q.; Zhang, Y.; Hu, J.; Zhang, D.; Zhou, S.; Zhao, X.; Zhang, J.; Zhu, Z.; et al. Ultrasensitive xylene gas sensor based on flower-like SnO_2/Co_3O_4 nanorods composites prepared by facile two-step synthesis method. *Nanotechnology* **2020**, *31*, 255501. [CrossRef] [PubMed]
7. Gao, H.Y.; Yu, Q.; Chen, K.; Sun, P.; Liu, F.M.; Yan, X.; Liu, F.M.; Lu, G.Y. Ultrasensitive gas sensor based on hollow tungsten trioxide-nickel oxide (WO_3-NiO) nanoflowers for fast and selective xylene detection. *J. Colloid Interface Sci.* **2019**, *535*, 458–468. [CrossRef]
8. Guo, M.M.; Luo, N.; Chen, Y.; Fan, Y.; Wang, X.H.; Xu, J.Q. Fast-response MEMS xylene gas sensor based on CuO/WO_3 hierarchical structure. *J. Hazard. Mater.* **2022**, *429*, 127471. [CrossRef] [PubMed]
9. Gao, H.; Wei, D.; Lin, P.; Liu, C.; Sun, P.; Shimanoe, K.; Yamazoe, N.; Lu, G. The design of excellent xylene gas sensor using Sn-doped NiO hierarchical nanostructure. *Sens. Actuators B Chem.* **2017**, *253*, 1152–1162. [CrossRef]

10. Li, D.K.; He, B.Y.; Chen, K.Q.; Pi, M.Y.; Cui, Y.T.; Zhang, D.K. Xylene gas sensing performance of Au nanoparticles loaded WO_3 nanoflowers. *Acta Phys. Sin.* **2019**, *68*, 198101. [CrossRef]
11. Wang, Q.J.; Li, C.Y.; Sun, P.; Liu, F.M.; Lu, G.Y.; Li, X. Hydrothermal and sintering synthesis of porous sheet-like NiO for xylene gas sensor. *Mater. Res. Express* **2019**, *6*, 1150e6. [CrossRef]
12. Meng, F.; Wang, H.; Yuan, Z.; Zhang, R.; Li, J. Ppb-Level Triethylamine Gas Sensors Based on Palladium Nanoparticles Modified Flower-Like In_2O_3 Grown on rGO Nanosheets Operating at Low Temperature. *IEEE Trans. Instrum. Meas.* **2022**, *71*, 9507909. [CrossRef]
13. Ji, H.; Qin, W.; Yuan, Z.; Meng, F. Qualitative and quantitative recognition method of drug-producing chemicals based on SnO_2 gas sensor with dynamic measurement and PCA weak separation. *Sens. Actuators B Chem.* **2021**, *348*, 130698. [CrossRef]
14. Meng, F.; Shi, X.; Yuan, Z.; Ji, H.; Qin, W.; Shen, Y.; Xing, C. Detection of four alcohol homologue gases by ZnO gas sensor in dynamic interval temperature modulation mode. *Sens. Actuators B Chem.* **2022**, *350*, 130867. [CrossRef]
15. Meng, F.L.; Qi, T.Y.; Zhang, J.J.; Zhu, H.M.; Yuan, Z.Y.; Liu, C.Y.; Qin, W.B.; Ding, M.N. MoS_2-Templated Porous Hollow MoO_3 Microspheres for Highly Selective Ammonia Sensing via a Lewis Acid-Base Interaction. *IEEE Trans. Ind. Electron.* **2022**, *69*, 960–970. [CrossRef]
16. Singh, K.J.; Singh, R.C. Enhanced toluene sensing performance of nanostructured aluminium-doped nickel oxide gas sensor. *Appl. Phys. A Mater. Sci. Process.* **2023**, *129*, 263. [CrossRef]
17. Gao, H.; Zhao, L.; Wang, L.; Sun, P.; Lu, H.; Liu, F.; Chuai, X.; Lu, G. Ultrasensitive and low detection limit of toluene gas sensor based on SnO_2-decorated NiO nanostructure. *Sens. Actuators B Chem.* **2018**, *255*, 3505–3515. [CrossRef]
18. Bai, G.; Dai, H.; Deng, J.; Liu, Y.; Ji, K. Porous NiO nanoflowers and nanourchins: Highly active catalysts for toluene combustion. *Catal. Commun.* **2012**, *27*, 148–153. [CrossRef]
19. Shang, W.; Wang, D.; Zhang, B.; Jiang, C.; Qu, F.; Yang, M. Aliovalent Fe(III)-doped NiO microspheres for enhanced butanol gas sensing properties. *Dalton Trans.* **2018**, *47*, 15181–15188. [CrossRef]
20. Wang, S.; Huang, D.; Xu, S.; Jiang, W.; Wang, T.; Hu, J.; Hu, N.; Su, Y.; Zhang, Y.; Yang, Z. Two-dimensional NiO nanosheets with enhanced room temperature NO_2 sensing performance: Via Al doping. *Phys. Chem. Chem. Phys.* **2017**, *19*, 19043–19049. [CrossRef]
21. Zhou, L.; Zeng, W.; Li, Y. A facile one-step hydrothermal synthesis of a novel NiO/ZnO nanorod composite and its enhanced ethanol sensing property. *Mater. Lett.* **2019**, *254*, 92–95. [CrossRef]
22. Wang, C.; Cui, X.B.; Liu, J.Y.; Zhou, X.; Cheng, X.Y.; Sun, P.; Hu, X.L.; Li, X.W.; Zheng, J.; Lu, G.Y. Design of Superior Ethanol Gas Sensor Based on Al-Doped NiO Nanorod-Flowers. *ACS Sens.* **2016**, *1*, 131–136. [CrossRef]
23. Bai, G.; Dai, H.; Deng, J.; Liu, Y.; Qiu, W.; Zhao, Z.; Li, X.; Yang, H. The microemulsion preparation and high catalytic performance of mesoporous NiO nanorods and nanocubes for toluene combustion. *Chem. Eng. J.* **2013**, *219*, 200–208. [CrossRef]
24. Park, S.; Kim, S.; Sun, G.J.; Lee, C. NO_2 Gas Sensing Performance of Co-Doped NiO Thin Film Sensors. *Nanosci. Nanotechnol. Lett.* **2015**, *7*, 713–717. [CrossRef]
25. Park, J.Y.; Choi, S.W.; Jung, S.H.; Kim, S.S. Synthesis of NiO Nanofibers and Their Gas Sensing Properties. *J. Nanosci. Nanotechnol.* **2012**, *12*, 1288–1291. [CrossRef] [PubMed]
26. Feng, C.H.; Wang, C.; Zhang, H.; Li, X.; Wang, C.; Cheng, P.F.; Ma, J.; Sun, P.; Gao, Y.; Zhang, H.; et al. Enhanced sensitive and selective xylene sensors using W-doped NiO nanotubes. *Sens. Actuators B Chem.* **2015**, *221*, 1475–1482. [CrossRef]
27. Chen, H.; Ao, S.R.; Li, G.D.; Gao, Q.; Zou, X.X.; Wei, C.D. Enhanced sensing performance to toluene and xylene by constructing $NiGa_2O_4$-NiO heterostructures. *Sens. Actuators B Chem.* **2019**, *282*, 331–338. [CrossRef]
28. Cao, J.; Wang, Z.Y.; Wang, R.; Zhang, T. Electrostatic sprayed Cr-loaded NiO core-in-hollow-shell structured micro/nanospheres with ultra-selectivity and sensitivity for xylene. *Crystengcomm* **2014**, *16*, 7731–7737. [CrossRef]
29. Wang, D.Y.; Mi, Q.; Zhang, H.; Li, G.L.; Zhang, D.Z. Sensitive Xylene Gas Sensor Based on NiO-$NiCo_2O_4$ Hierarchical Spherical Structure Constructed with Nanorods. *IEEE Sens. J.* **2022**, *22*, 10346–10352. [CrossRef]
30. Qin, W.; Yuan, Z.; Gao, H.; Zhang, R.; Meng, F. Perovskite-structured $LaCoO_3$ modified ZnO gas sensor and investigation on its gas sensing mechanism by first principle. *Sens. Actuators B Chem.* **2021**, *341*, 130015. [CrossRef]
31. Wang, F.; Bai, S.; Tress, W.; Hagfeldt, A.; Gao, F. Defects engineering for high-performance perovskite solar cells. *Npj Flex. Electron.* **2018**, *2*, 22. [CrossRef]
32. Park, N.G. Perovskite solar cells: An emerging photovoltaic technology. *Mater. Today* **2015**, *18*, 65–72. [CrossRef]
33. Zhang, H.; Nazeeruddin, M.K.; Choy, W.C.H. Perovskite Photovoltaics: The Significant Role of Ligands in Film Formation, Passivation, and Stability. *Adv. Mater.* **2019**, *31*, 1805702. [CrossRef]
34. Pham, T.T.; Shin, E.W. Influence of g-C_3N_4 Precursors in g-C_3N_4/$NiTiO_3$ Composites on Photocatalytic Behavior and the Interconnection between g-C_3N_4 and $NiTiO_3$. *Langmuir* **2018**, *34*, 13144–13154. [CrossRef]
35. Jin, Y.M.; Shen, X.F.; Liu, Z.X.; Wang, Z.J.; Zhu, B.; Xu, P.F.; Luo, L.; Zhang, L. Synthesis of $NiTiO_3$-Bi_2MoO_6 core-shell fiber-shaped heterojunctions as efficient and easily recyclable photocatalysts. *New J. Chem.* **2018**, *42*, 411–419. [CrossRef]
36. Wang, J.; Liu, A.; Wang, C.; You, R.; Liu, F.; Li, S.; Yang, Z.; He, J.; Yan, X.; Sun, P.; et al. Solid state electrolyte type gas sensor using stabilized zirconia and $MTiO_3$ (M: Zn, Co and Ni)-SE for detection of low concentration of SO_2. *Sens. Actuators B Chem.* **2019**, *296*, 126644. [CrossRef]
37. Li, F.; Guo, S.J.; Shen, J.L.; Shen, L.; Sun, D.M.; Wang, B.; Chen, Y.; Ruan, S.P. Xylene gas sensor based on Au-loaded WO_3 center dot H_2O nanocubes with enhanced sensing performance. *Sens. Actuators B Chem.* **2017**, *238*, 364–373. [CrossRef]

38. Xu, Y.; Tian, X.; Fan, Y.; Sun, Y. A formaldehyde gas sensor with improved gas response and sub-ppm level detection limit based on NiO/$NiFe_2O_4$ composite nanotetrahedrons. *Sens. Actuators B Chem.* **2020**, *309*, 127719. [CrossRef]
39. Zhou, Q.; Zeng, W.; Chen, W.; Xu, L.; Kumar, R.; Umar, A. High sensitive and low-concentration sulfur dioxide (SO_2) gas sensor application of heterostructure NiO-ZnO nanodisks. *Sens. Actuators B Chem.* **2019**, *298*, 126870. [CrossRef]
40. Bai, S.; Zhang, K.; Zhao, Y.; Li, Q.; Luo, R.; Li, D.; Chen, A. rGO decorated NiO-$BiVO_4$ heterojunction for detection of NO_2 at low temperature. *Sens. Actuators B Chem.* **2021**, *329*, 128912. [CrossRef]
41. Perrone, O.M.; Roveda, A.C.; de Moraes, D.A.; Volanti, D.P. The enhanced n-butanol sensing performance of In_2O_3 loaded NiO cuboid heterostructure. *J. Alloys Compd.* **2023**, *930*, 167483. [CrossRef]
42. Zhang, Y.Q.; Bai, J.H.; Zhou, L.S.; Liu, D.Y.; Liu, F.M.; Liang, X.S.; Gao, Y.; Liu, F.M.; Yan, X.; Lu, G.Y. Preparation of silver-loaded titanium dioxide hedgehog-like architecture composed of hundreds of nanorods and its fast response to xylene. *J. Colloid Interface Sci.* **2019**, *536*, 215–223. [CrossRef] [PubMed]
43. Zhu, B.L.; Zeng, D.W.; Wu, J.; Song, W.L.; Xie, C.S. Synthesis and gas sensitivity of In-doped ZnO nanoparticles. *J. Mater. Sci. Mater. Electron.* **2003**, *14*, 521–526. [CrossRef]
44. Jiang, D.; Wei, W.; Li, F.; Li, Y.; Liu, C.; Sun, D.; Feng, C.; Ruan, S. Xylene gas sensor based on α-MoO_3/α-Fe_2O_3 heterostructure with high response and low operating temperature. *RSC Adv.* **2015**, *5*, 39442–39448. [CrossRef]
45. Lin, Z.X.; Gong, J.M.; Fu, P. Hierarchical Fe_2O_3/Bi_2WO_6 nanoplates with enhanced xylene sensing performance. *J. Mater. Sci. Mater. Electron.* **2017**, *28*, 4424–4430. [CrossRef]